Bubble nuclei within the self-consistent Hartree-Fock mean field plus pairing approach

L. Tan Phuc,[1,2,*] N. Quang Hung,[1,†] and N. Dinh Dang[3,4,‡]

[1]*Institute of Fundamental and Applied Sciences, Duy Tan University, 3 Quang Trung, Danang City 550000, Vietnam*

[2]*Faculty of Physics and Engineering Physics, Vietnam National University Ho Chi Minh City-University of Science, Ho Chi Minh 748355, Vietnam*

[3]*Quantum Hadron Physics Laboratory, RIKEN Nishina Center for Accelerator-Based Science, 2-1 Hirosawa, Wako City, 351-0198 Saitama, Japan*

[4]*Institute for Nuclear Science and Technique, Hanoi, 122100 Vietnam*

(Received 12 December 2017; published 23 February 2018)

The depletion of the nuclear density at its center, called the nuclear bubble, is studied within the Skyrme Hartree-Fock mean field consistently incorporating the superfluid pairing. The latter is obtained within the finite-temperature Bardeen-Cooper-Schrieffer theory and within the approach using the exact pairing. The numerical calculations are carried out for ^{22}O and ^{34}Si nuclei, whose bubble structures, caused by a very low occupancy of the $2s_{1/2}$ level, were previously predicted at $T = 0$. Among 24 Skyrme interactions under consideration, the MSk3 is the only one which reproduces the experimentally measured occupancy of the $2s_{1/2}$ proton level as well as the binding energy, and consequently produces the most pronounced bubble structure in ^{34}Si. As compared to the approaches employing the same BSk14 interaction, our approach with exact pairing predicts a pairing effect which is stronger in ^{22}O and weaker in ^{34}Si. The increase in temperature depletes the bubble structure and completely washes it out when the temperature reaches a critical value, at which the factor measuring the depletion of the nucleon density vanishes.

DOI: 10.1103/PhysRevC.97.024331

I. INTRODUCTION

The depletion of the nucleon density at the center of an atomic nucleus was first proposed by Wilson in 1946, who employed a classical oscillation of the spherical shell (bubble) to describe the low-lying excited states in spherical nuclei [1]. Siemens and Bethe also discussed the existence of stable spherical shells [2]. The first microscopic model of the bubble structure was presented by Campi and Sprung in 1973 [3], initiating many works by other authors ever since [4–11]. In recent years, the study of the nuclear bubble structure was extended to superheavy and hyperheavy nuclei [12–17].

The depletion of the nuclear density at its center is characterized by the absence of the s-orbital wave function. A special character of the s-radial wave is a pronounced maximum, which is located at the nuclear center ($r = 0$). Therefore, the s-radial wave is expected to significantly contribute to the nuclear density distribution at $r = 0$ and the absence of the s wave is the main reason causing the bubble structure in the nuclear density at its center. An example is seen in the electron scattering on ^{206}Pb and ^{205}Tl, where the ground state and excited states of ^{205}Tl are described as three-hole states, which consist of one proton hole $(3s_{1/2})_Z^{-1}$ and two neutron holes $(2d_{3/2})_N^{-2}$, with respect to the closed shell ^{208}Pb [18,19]. These experiments confirmed the theoretical predictions [20] that the single-particle strength of the proton-hole configuration $3s_{1/2}$ in ^{205}Tl amounts to 70%–90%, whereas the remaining strength of 30%–10% is mainly exhausted in the two-neutron hole configuration $2d_{3/2}$ [18]. This indicates that the candidates to the bubble structure must have unoccupied s levels, such as ^{22}O and ^{34}Si (unoccupied $2s$ level) [9,11], ^{46}Ar (unoccupied $2s$ level) [8,21], and ^{206}Hg (unoccupied $3s$ level) [21]. In these bubble candidates, the shell closure often takes place when the states of low angular momenta are located at or near the top of the Fermi energy. In the case of a bubble structure, the energies of these states increase in such a way that they become unoccupied and are located at appreciably higher energies as compared to the adjacent lower states, creating new magic numbers [5]. Several "bubble magic numbers" were proposed by Wong [4,5] and Campi [3] as 18, 34, 50, 58, 70, 80, 120. These nuclei were called the possible bubble nuclei. Some among them, such as ^{36}Ar and ^{200}Hg [3,4], have been turned down in later calculations and experiments [10,22] because of strong correlations (such as pairing and deformation). To ensure the low occupancy of s levels for the bubble structure to take place, the pairing correlation and deformation should be weak [23]. Therefore, the optimal bubble candidates are the spherical nuclei with shell closures at unoccupied s levels. These nuclei must have the s-single-particle level separated from those around it to reduce the correlations. Some good neutron and proton bubble candidates are ^{22}O ($N = 14$, $Z = 8$) and ^{34}Si ($N = 20$, $Z = 14$), respectively. For ^{22}O, the neighboring isotope ^{24}O, which can be referred to as its adjoint candidate, is used to investigate the depletion of the neutron density in the interior of ^{22}O because ^{24}O has two neutrons filling the $2s_{1/2}$ level, which is empty in ^{22}O. This

*letanphuc191190@gmail.com
†nqhungdtu@gmail.com
‡dang@riken.jp

 ©2018 American Physical Society

makes ^{22}O a good bubble candidate. The depletion factor was predicted to be around 24%–28% for ^{22}O [9]. With the same structure, an excellent candidate for the proton bubble is ^{34}Si, whose adjoint candidate is ^{36}S ($Z = 16$, $N = 20$). The neutron shells of ^{34}Si are sufficiently tight to prevent the coupling and correlation effects. The observation of proton densities in ^{34}Si and ^{36}S would demonstrate the importance of s-orbital contributions. In Ref. [9] three different models, namely the shell, relativistic, and nonrelativistic mean-field models, were used to predict the proton bubble in ^{34}Si. The results showed that the depletion of proton and charge densities are about 40% and 25%, respectively. The occupancy of the $2s_{1/2}$ level was predicted to be around ∼0.08, which reinforces the belief that the existence of the proton bubble in this nucleus is very likely. Most recently, the occupancy of the $2s_{1/2}$ level in ^{34}Si was measured in Ref. [24] to be 0.17 ± 0.03, which serves as useful information for simulating the bubble structure in this nucleus by using different microscopic models.

The bubble structure in low-lying excited states was investigated by Yao [25], where a relativistic version of configuration mixing of both particle-number and angular-momentum projected quadrupole deformed mean-field states was used to study the possible existence of the proton bubble in ^{34}Si in the low-lying states. Pairing correlations and nuclear fluctuations were included in the calculations. The results showed that the proton bubble in these states is very unlikely. However, the occupancy of $s_{1/2}$ levels, which play an important role in the description of the central nuclear density, remains unknown. Any effect which alters the occupancy, such as the pairing correlations [3,9,10,26] and shape fluctuations [10], must be taken into account, but they cannot sufficiently quench the bubble structure at zero temperature ($T = 0$) [8]. In general, the correlations tend to flatten the density distribution [10].

In the present work we will study the bubble structures in two spherical nuclei, namely ^{22}O and ^{34}Si, at zero temperature as well as their evolution as a function of temperature. This is performed by using a Skyrme interaction and pairing strength that reproduce the binding and two-proton separation energies as well as the experimentally measured occupancy of the $2s_{1/2}$ level in ^{34}Si at $T = 0$ [24]. For ^{22}O, because the experimental occupancy of the $2s_{1/2}$ level is not available, we use the same Skyrme interaction, which is employed in the calculations for ^{34}Si, and adjust the pairing strength to reproduce the binding and two-neutron separation energies. The candidate nuclei are treated in the Hartree-Fock (HF) method with temperature-dependent densities plus temperature-dependent pairing correlation in a consistent way. The latter is taken into account by using the finite-temperature Bardeen-Cooper-Schrieffer (FTBCS) theory and the approach which incorporates the exact eigenvalues of the pairing problem in the canonical ensemble (CE). The density-dependent Skyrme interactions are used to calculate the single-particle spectra in the nuclear mean fields, which are expected to be better as compared to those obtained by using the density-independent interactions [3]. On the other hand, Skyrme interactions also include the spin-orbit terms [27,28], which are stronger at low j momenta towards the nuclear center and weaker at the nuclear surface [21]. Hence the depletion of the spin-orbit splitting around the nuclear center can be explained by the bubble structure [10,25]. The results obtained at $T = 0$ within the present work are also compared with the predictions by the Hartree-Fock-Bogolyubov (HFB) approach [9,11,29].

The paper is organized as follows. The formalism of the finite-temperature Hartree-Fock (FTHF) and finite-temperature exact pairing (FTEP) methods are reported in Sec. II. The results of numerical calculations are analyzed in Sec. III. The paper is summarized in the last section, where conclusions are drawn.

II. FORMALISM

A. Finite temperature Hartree-Fock (FTHF) method

The Hartree-Fock method at $T = 0$ considers a nuclear Hamiltonian in the form [28],

$$\hat{H} = \sum_i \hat{t}_i + \sum_{i<j} v_{ij} + \sum_{i<j<k} v_{ijk}, \tag{1}$$

where $\hat{t}_i$ is the kinetic energy operator; v_{ij} and v_{ijk} are two- and three-body interactions, respectively. By using the density-dependent nucleon-nucleon interaction given in the form of the Skyrme interaction, the two-body and three-body terms can be explicitly written as [27,28]

$$\begin{aligned} v_{ij} &= t_0(1 + x_0 P_\sigma)\delta(\vec{r}) + \tfrac{1}{2}t_1[\delta(\vec{r})\vec{k}^2 + \vec{k'}^2\delta(\vec{r})] \\ &\quad + t_2\vec{k'}\delta(\vec{r})\vec{k} + iW_0(\vec{\sigma_i} + \vec{\sigma_j})\vec{k} \times \delta(\vec{r})\vec{k}, \end{aligned} \tag{2}$$

$$v_{ijk} = t_3\delta(\vec{r_i} - \vec{r_j})\delta(\vec{r_j} - \vec{r_k}), \tag{3}$$

where $\vec{r} = \vec{r_i} - \vec{r_j}$, $\vec{k} = \frac{1}{2}(\nabla_i - \nabla_j)$, $\vec{k'}$ is the conjugate of $\vec{k}$, and $P_\sigma = \frac{1}{2}(1 + \sigma_i\sigma_j)$ is the spin-exchange operator with $\sigma_{i(j)}$ being the Pauli matrix. The three-body interaction can be approximately expressed in terms of the two-body one by using the nucleon density,

$$v_{ijk} \longrightarrow v_{ij} = \frac{t_3}{6}(1 + P_\sigma)\delta(\vec{r_i} - \vec{r_j})\rho^\alpha\left(\frac{\vec{r_i} - \vec{r_j}}{2}\right), \tag{4}$$

where the total nuclear density $\rho = \rho_Z + \rho_N$ is the sum of the proton and neutron densities, ρ_Z and ρ_N, respectively.

The derivation of the Skyrme Hartree-Fock equations was described in detail, e.g., in Ref. [28], so we report here only its final equation in the coordinate space as

$$\begin{aligned} &\left[-\nabla\frac{\hbar^2}{2m^*(\vec{r})}\nabla + U(\vec{r}) + U_{\rm Coul}(\vec{r}) + \frac{1}{i}W(\vec{r})(\nabla \times \sigma)\right]\varphi_j(\vec{r}) \\ &= \epsilon_j\varphi_j(\vec{r}), \end{aligned} \tag{5}$$

where $m^*(\vec{r})$ is the effective mass, whereas $U(\vec{r})$, $U_{\rm Coul}(\vec{r})$, and $W(\vec{r})$ are the Skyrme, Coulomb, and spin-orbit potentials, respectively. To obtain the wave functions φ_j and energies ϵ_j of the single-particle levels, the HF equation (5) is often being solved by using the currents and densities of the form [30],

$$\rho_q(r) = \sum_j f_j\frac{2j+1}{4\pi}\varphi_j(r)^2, \tag{6}$$

$$\tau_q(r) = \sum_j f_j\frac{2j+1}{4\pi}\left[[\partial_r\varphi_j(r)]^2 + \frac{l(l+1)}{r^2}\varphi_j(r)^2\right], \tag{7}$$

$$J_q(r) = \sum_j f_j\frac{2j+1}{4\pi}\left[j(j+1) - l(l+1) - \frac{3}{4}\right]\frac{2}{r}\varphi_j(r)^2, \tag{8}$$

where f_j are the occupation numbers of the corresponding single-particle levels j, and the sums are carried out separately over the proton or neutron levels. Within the HF approach at $T = 0$, the single-particle occupation numbers f_j of the levels below the Fermi one are always equal to 1, and those above it are zero. In other words, the levels j with $\epsilon_j < \epsilon_F$ are fully occupied, and those with $\epsilon_j > \epsilon_F$ are empty. Therefore, Eqs. (6)–(8) contain only occupied levels $\epsilon_j < \epsilon_F$ (ϵ_F is the Fermi energy). At finite temperature ($T \neq 0$), instead of being evaluated in the ground state, the expectation values in the HF equation are taken in the grand canonical ensemble (GCE), resulting in the single-particle occupation numbers in terms of the Fermi-Dirac distribution as

$$f_j = \frac{1}{e^{(\epsilon_j - \lambda)/T} + 1}. \tag{9}$$

The temperature-dependent chemical potential λ (distorted Fermi level) is found by solving the equation for the particle number,

$$N = 2\sum_j \Omega_j f_j, \quad \Omega_j = j + 1/2, \tag{10}$$

for proton (Z) or neutron (N) numbers, separately. Therefore, at $T \neq 0$, the HF single-particle spectra consist of single-particle levels below as well as above λ. The levels with $\epsilon_j > \lambda$ are obtained by discretizing the continuum [31]. The set of Eqs. (5)–(9) forms the FTHF equations. By solving them, one obtains the temperature-dependent single-particle spectra ϵ_j, wave functions φ_j, and occupation numbers f_j.

B. Pairing effect in hot nuclei

Pairing plays an important role in nuclei, in particular in the neutron-rich ones, where a strong pairing effect was observed [32–34]. It is the source of the odd-even staggering effect, which affects the single-particle occupancies, single-particle spectra, nuclear level density, nuclear binding energy, and nucleon separation energy [33,35,36]. In ground-state (cold) nuclei, that is, nuclei at $T = 0$, pairing is often described approximately within the BCS theory [37] or exactly by using the exact eigenvalues of the pairing problem, which can be obtained, for example, by diagonalizing the pairing Hamiltonian [33,34]. In highly excited nuclei, such as nuclei at $T \neq 0$ (hot nuclei), the temperature effect breaks the nucleon pairs, leading to the quenching of pairing as T increases [38–40]. The approaches using the BCS and exact pairing (EP) formalisms at $T \neq 0$ are summarized below.

1. *The finite-temperature BCS (FTBCS) theory*

The present paper considers a pairing Hamiltonian of the form [28],

$$\hat{H} = \sum_j \epsilon_j a^\dagger_{jm} a_{jm} - G \sum_{mm'} a^\dagger_{jm} a^\dagger_{j\tilde{m}} a_{j'\tilde{m}'} a_{j'm'}, \tag{11}$$

where $a^\dagger_{jm}$ and a_{jm} are the creation and annihilation operators of a nucleon moving on the jth orbitals with projections $\pm m$ and degeneracies $\Omega_j = j + 1/2$ and the single-particle energy ϵ_j. The symbol $\tilde{}$ denotes the time-reversal operator $a_{j\tilde{m}} = (-1)^{j-m} a_{j-m}$. This pairing Hamiltonian (11) describes a system of N neutrons and Z protons interacting via a monopole-pairing interaction with a constant pairing interaction G. The FTBCS equations are conventionally obtained by applying the variational procedure to minimize the expectation value of the Hamiltonian $\mathcal{H} = H - \lambda\hat{N}$ within the GCE [41], where $\hat{N} = \sum_{jm} a^\dagger_{jm} a_{jm}$ is the particle-number operator and λ is the chemical potential. The explicit form of the FTBCS equations for the pairing gap Δ and particle number N is then given as

$$\Delta = G\sum_j \Omega_j u_j v_j (1 - 2n_j), \tag{12}$$

$$N = 2\sum_j \Omega_j \left[n_j u_j^2 + (1 - n_j) v_j^2\right], \tag{13}$$

where the coefficients u_j and v_j of the Bogolyubov transformation from the particles to the quasiparticles read

$$u_j^2 = \frac{1}{2}\left(1 + \frac{\epsilon_j - \lambda}{E_j}\right), \quad v_j^2 = 1 - u_j^2, \tag{14}$$

with the quasiparticle energies E_j and quasiparticle occupation numbers n_j defined as

$$E_j = \sqrt{(\epsilon_j - \lambda)^2 + \Delta^2}, \tag{15}$$

$$n_j = \frac{1}{e^{E_j/T} + 1}. \tag{16}$$

Within the FTBCS, the single-particle occupation numbers f_j in the HF densities (6)–(8) are expressed in terms of the Bogolyubov coefficients u_j, v_j and quasiparticle occupation numbers n_j as

$$f_j = n_j u_j^2 + (1 - n_j) v_j^2. \tag{17}$$

The major drawback of the BCS theory is that it conserves the particle number only in average $N = \langle\hat{N}\rangle$. At $T \neq 0$, the FTBCS gap collapses at a certain critical temperature $T_c \sim 0.57\Delta(T = 0)$, signalizing the transition from the superfluid phase to the normal one. However, various approximations beyond the FTBCS have already shown that thermal fluctuations in finite systems as atomic nuclei smooth out this phase transition, resulting in a thermal gap, which does not vanish at $T \geqslant T_c$, but monotonically decreases with increasing T (see, e.g., Refs. [40–45]).

2. *Exact pairing at finite temperature (FTEP)*

Based on the SU(2) algebra of angular momentum, the pairing Hamiltonian (11) can be directly diagonalized to obtain the exact eigenstates $\mathcal{E}_S$ and single-particle occupation numbers f_j^S at $T = 0$ and at different values of the total seniority S, which is the total number of unpaired particles [33,34]. Using these eigenvalues, one can construct the exact partition function within the CE as [40,46]

$$Z(T) = \sum_S 2^S e^{-\mathcal{E}_S/T}. \tag{18}$$

Knowing the partition function, one can easily calculate all the thermodynamic quantities including the free energy $\mathcal{F}$, total

energy $\mathcal{E}$, heat capacity $\mathcal{C}$, and pairing gap Δ as

$$\mathcal{F} = -T\ln Z(T), \quad \mathcal{S} = -\frac{\partial \mathcal{F}}{\partial T}, \tag{19}$$

$$\mathcal{E} = \mathcal{F} + T\mathcal{S}, \quad \mathcal{C} = \frac{\partial \mathcal{E}}{\partial T}, \tag{20}$$

$$\Delta = \sqrt{-G\mathcal{E}_{\rm pair}}, \quad \mathcal{E}_{\rm pair} = \mathcal{E} - 2\sum_j \Omega_j \left[\epsilon_j - \frac{G}{2} f_j\right] f_j, \tag{21}$$

where the temperature-dependent single-particle occupation numbers f_j are calculated from the state-dependent occupation numbers f_j^S as

$$f_j = \frac{1}{Z}\sum_S 2^S f_j^{(S)} e^{-\mathcal{E}_S/T}. \tag{22}$$

Within the FTEP, the particle number is exactly conserved at both zero and finite temperatures. As a result, the exact pairing gap does not vanish at $T = T_c$ as the FTBCS gap but monotonically decreases with increasing T and remains finite at T as high as 4 MeV [40,46].

C. Nucleon density

The procedure of solving the FTHF, FTBCS, and FTEP equations, making use of the HF single-particle spectra, is explained as follows. First, the HF equation (5) is solved at $T = 0$ to obtain all the occupied and unoccupied single-particle levels. These single-particle energies are then used in solving the FTHF, FTBCS, and FTEP equations to obtain the corresponding single-particle occupation numbers $f_j^{\rm FTHF}$ [Eq. (9)], $f_j^{\rm FTBCS}$ [Eq. (17)], and $f_j^{\rm FTEP}$ [Eq. (22)] at a given T. The obtained temperature-dependent occupation numbers are used to calculate the HF currents and densities (6)–(8), which are now temperature dependent. By using these temperature-dependent currents and densities, one can solve the HF equation (5) again to obtain the new single-particle spectra ϵ_j and wave functions $\varphi_j(r)$, which are also temperature dependent. These new spectra and wave functions are then used to obtain the single-particle occupation numbers $f_j^{\rm FTHF}, f_j^{\rm FTBCS}$, and $f_j^{\rm FTEP}$ by solving the FTHF, FTBCS, and FTEP equations. The process is repeated until the convergence is reached. It is worth mentioning here that, within the FTEP, the exact diagonalization of the pairing Hamiltonian is limited to a truncated spectrum of single-particle levels around the Fermi surface because of the limitation in the size of the matrix to be diagonalized [40]. (The effect of the configurational truncation in the exact solution of the pairing problem was thoroughly discussed in Refs. [47,48]). The levels outside the truncated spectrum are treated within the independent particle model (IPM), whose occupation numbers are expressed in terms of the Fermi-Dirac distribution as in the case of the FTHF [Eq. (9)] [46]. Regarding the FTHF and FTBCS cases, in general, no cutoff is required as the matrix diagonalization is not used in solving them. However, to be consistent and physically meaningful, we also use the same truncated single-particle spectrum for the FTBCS as that employed for the FTEP.

TABLE I. Occupation numbers $f_{2s_{1/2}}$ of the $2s_{1/2}$ level, pairing gaps Δ, and depletion factors F of ^{22}O and ^{34}Si obtained by using different Skyrme interactions within the FTEP at $T = 0$.

Interaction	^{34}Si			^{22}O		
	$f_{2s_{1/2}}$	Δ_Z	$F(\%)$	$f_{2s_{1/2}}$	Δ_N	$F(\%)$
MSk1	0.096	1.35	17	0.203	1.15	2
MSk2	0.129	1.67	15	0.241	1.34	1
MSk3	0.090	1.34	19	0.247	1.54	2
MSk4	0.125	1.68	16	0.280	1.70	0
MSk5	0.126	1.69	16	0.279	1.69	0
MSk6	0.149	2.03	15	0.280	1.77	0
MSk7	0.154	2.10	15	0.285	1.82	0
MSk8	0.163	2.08	14	0.308	1.87	0
MSk9	0.136	1.94	16	0.275	1.78	1
BSk1	0.183	2.50	13	0.321	2.17	0
BSk2	0.171	2.40	12	0.252	1.58	1
BSk3	0.186	2.43	10	0.273	1.58	0
BSk4	0.120	2.01	15	0.169	1.25	6
BSk5	0.140	2.28	14	0.176	1.30	5
BSk6	0.106	2.09	18	0.165	1.51	7
BSk7	0.291	8.35	1	0.319	5.89	2
BSk8	0.198	3.79	12	0.282	2.82	2
BSk9	0.208	3.78	10	0.288	2.73	2
BSk10	0.209	3.28	8	0.282	2.10	1
BSk11	0.144	2.15	12	0.184	1.19	4
BSk12	0.137	2.05	13	0.178	1.14	4
BSk13	0.136	1.99	13	0.188	1.16	4
BSk14	0.122	2.18	14	0.140	1.14	7
BSk18	0.278	5.56	3	0.364	4.21	0

After solving the FTHF, FTBCS, and FTEP equations, one obtains the temperature-dependent single-particle spectra ϵ_j, occupation numbers f_j, and wave functions $\varphi_j(r)$ for neutrons and protons. The nucleon density is then calculated as

$$\rho(r) = \frac{1}{2\pi}\sum_j \Omega_j f_j \varphi_j(r)^2. \tag{23}$$

These occupation numbers and densities will serve as indicators in the study of the bubble structure discussed in Sec. III.

D. Center-of-mass correction

Because the solutions of the HF equations (5) represent a localized mean field, the translational invariance is always broken within the HF, causing the oscillation of the nuclear center of mass in the mean field. To eliminate this oscillation one should project the exact ground state, that is, a state with good zero angular momentum, out of the given mean-field state. This complex task is often substituted with a simple subtraction of the zero-point energy $E_{\rm c.m.}$ of the center-of-mass (c.m.) quasiharmonic oscillation [30,49], which is estimated in terms of the momentum operators $\hat{p}$ and single-particle occupation

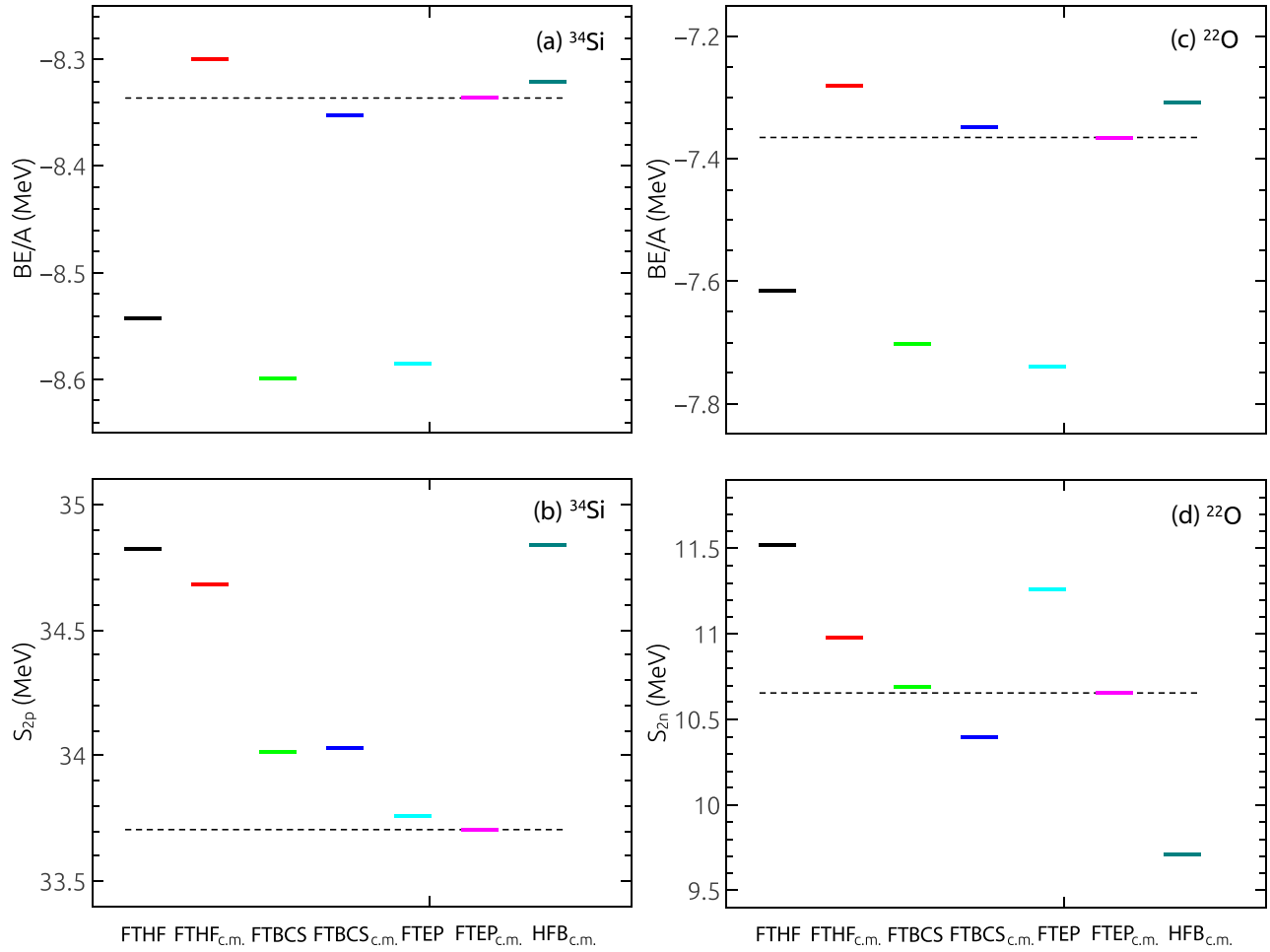

FIG. 1. Binding energy per nucleon BE/A and two proton (neutron) separation energy S_{2p} (S_{2n}) obtained from different methods using the MSk3 interaction at $T = 0$. The results of HFB with BSk14 are extracted from the mass excesses taken from RIPL3 [29]. The dashed lines represent the experimental data.

numbers f_j as

$$E_{\text{c.m.}} = \frac{\langle P^2_{\text{c.m.}} \rangle}{2Am}, \tag{24}$$

$$\langle P^2_{\text{c.m.}} \rangle = \sum_j f_j \langle \varphi_j | \hat{p}^2 | \varphi_j \rangle - \sum_{i,j} (f_i f_j + \sqrt{f_i(1-f_i) f_j (1-f_j)}) |\langle \varphi_i | \hat{p} | \varphi_j \rangle|^2. \tag{25}$$

where $P_{\text{c.m.}}$ is the total momentum operator, and A and m are the nucleon number and the average nucleon mass, respectively. The $E_{\text{c.m.}}$ correction is subtracted *a posteriori* from the total energy after variation of Hartree-Fock mean field following Refs. [30,50].

III. ANALYSIS OF NUMERICAL RESULTS

A. Ingredients of the numerical calculations

The numerical calculations are carried out within the FTHF, FTBCS, and FTEP for ^{22}O and ^{34}Si, whose bubble structures are predicted to be dominant at $T = 0$ [9]. As for the HF calculation, we employ the computer code, which was developed by Colò and collaborators [31]. We select two series of BSk [51–62] and MSk [63,64] interactions to make a test for ^{22}O and ^{34}Si because of the suitability of these interactions in the calculations with pairing [29,51–64]. These Skyrme interactions are tested within the HF plus exact pairing in combination with the full center-of-mass correction for the ground-state energy [50]. The value of the pairing strength G is adjusted to reproduce the experimental binding energies at $T = 0$ as follows.

Because ^{34}Si has the neutron closed shell, the pairing treatment within the FTBCS and FTEP is performed only for protons within a truncated spectrum around the Fermi surface, as was mentioned in Sec. II C, which includes seven proton levels with the $1d_{5/2}$ level located below the Fermi surface and the other six levels $2s_{1/2}$, $1d_{3/2}$, $1f_{7/2}$, $2p_{3/2}$, $1f_{5/2}$, and $2p_{1/2}$ above it. The remaining inner proton core is a closed-shell core with eight protons, so it does not contribute to the pairing correlation. The $2s_{1/2}$ level is the lowest unoccupied level above the Fermi one, whose occupancy was recently measured at $T = 0$ to be 0.17 ± 0.03 [24]. This very low occupancy of the

TABLE II. Values (%) of the depletion factor F for ^{22}O and ^{34}Si obtained from different methods at $T = 0$. The asterisk (*) denotes the methods used in the present work. The values of F within relativistic mean field (RMF), shell model (SM), and HFB are taken from Refs. [9,11,29].

Nucleus	FTHF* MSk3	FTBCS* MSk3	FTEP* MSk3	FTEP* BSk14	HFB [29] BSk14	HFB [29] D1S	HFB [9] SLy4	RMF [9] NL3	RMF+BCS [11] NL3	RMF [9] FSUGold	SM [9]
^{22}O	11%	2%	2%	7%	4%	4%	3%	28%	17%	34%	24%
^{34}Si	24%	19%	19%	14%	15%	28%	38%	37%	35%	42%	41%

$2s_{1/2}$ level is known to be the main source, causing a significant reduction in the s-wave function, which is the signature of the bubble structure in the proton density of ^{34}Si. As the $s_{1/2}$ level is doubly degenerated, its occupancy is twice the corresponding occupation number $f_{2s_{1/2}}$. The latter, therefore, is equal to half of the occupancy, namely $f_{2s_{1/2}} = 0.085 \pm 0.015$. The values of $f_{2s_{1/2}}$ in the interval $0.07 \leqslant f_j \leqslant 0.1$ shall be used as a criterion for choosing the suitable Skyrme interaction in the FTEP calculations. By varying the pairing interaction parameter G_Z for protons to reproduce the experimental binding energy per nucleon $BE/A = -8.336$ MeV, the FTEP, performed at $T = 0$ with the MSk3 interaction, also eventually produces the experimentally measured occupation number of the $2s_{1/2}$ level. The value of $G_Z = 0.547$ MeV obtained in this way is kept unchanged in the calculations at $T > 0$. The calculations within the BCS are also performed making use of the same value of the occupation number of $2s_{1/2}$ level. By doing so, we found the values of the FTBCS and FTEP pairing gaps at $T = 0$ to be 0.85 and 1.34 MeV, respectively. The two-proton separation energy $S_{2p} = B(N,Z) - B(N,Z-2)$ calculated in this process, with $B(N,Z)$ being the binding energy of a nucleus with N neutrons and Z protons, also reproduces well the experimental value $S_{2p} = 33.7$ MeV.

The ^{22}O nucleus ($Z = 8$ and $N = 14$) was predicted to have the neutron bubble structure at $T = 0$ [9,11]. Hence, the calculation is also carried out for seven selected neutron shells similar to those in ^{34}Si. Because we do not know the experimental occupancy of the $2s_{1/2}$ level at $T = 0$ for ^{22}O, we first choose the Skyrme interactions and the pairing parameter G_N for neutrons to reproduce the experimental binding energy per nucleon $BE/A = -7.365$ MeV. The occupation numbers of the $2s_{1/2}$ level and the pairing gaps, obtained in this way for ^{34}Si and ^{22}O by using 9 MSk and 15 BSk interactions are listed in Table I. The BSk15-BSk17 interactions failed to reproduce a good binding energy, so they are not shown in this table. For ^{22}O, we choose the MSk3 interaction to be consistent with that used for ^{34}Si. We also use the BSk14 interaction to compare the results of our calculations with those obtained within the HFB employing the same interaction [9,11,29].

Shown in Fig. 1 are the binding energies per nucleon BE/A and two proton (neutron) separation energies S_{2p} (S_{2n}) obtained within the FTHF, FTBCS, and FTEP methods by using the MSk3 interaction for ^{34}Si and ^{22}O at $T = 0$ without and including the center-of-mass correction. They are compared with the experimental data and also with the results of the HFB calculations by using the BSk14 interaction from Ref. [29]. This figure shows that the FTEP method including the center-of-mass correction is superior in describing the binding and two-nucleon separation energies. In particular, it indicates that the center-of-mass correction using the single-particle occupation numbers $f_j^{\rm FTEP}$ (22) supplied by the FTEP method plays a crucial role in reproducing the experimental values of the binding energy. The HFB results from Ref. [29] slightly overestimate the binding energies. However, as compared to the FTEP method including the center-of-mass correction,

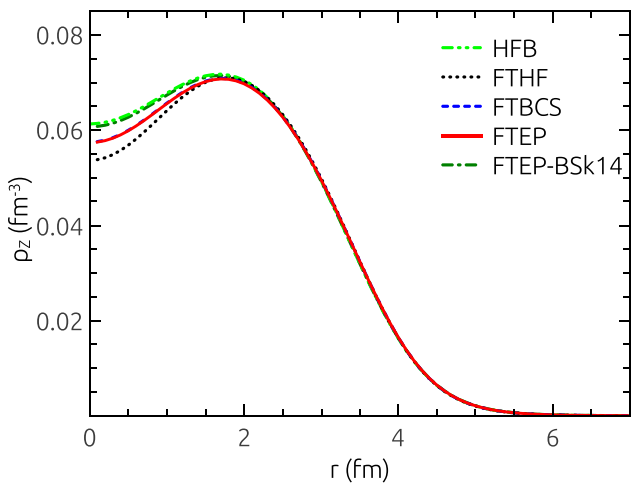

FIG. 2. Proton density $\rho_Z(r)$ for ^{34}Si obtained within the FTHF, FTBCS, FTEP, and HFB at $T = 0$.

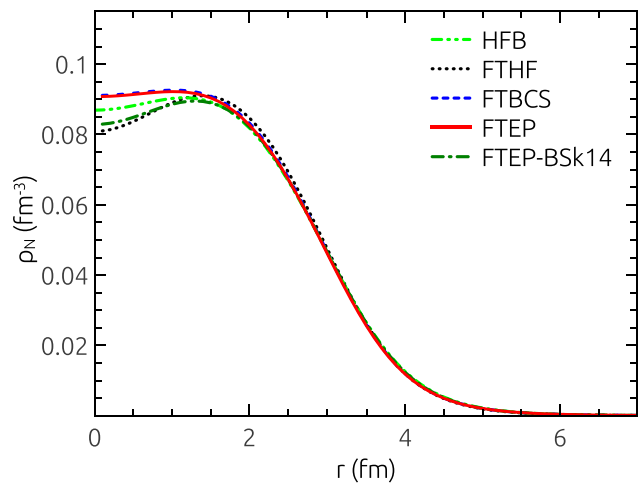

FIG. 3. Neutron density $\rho_N(r)$ for ^{22}O. Notations are the same as in Fig. 2.

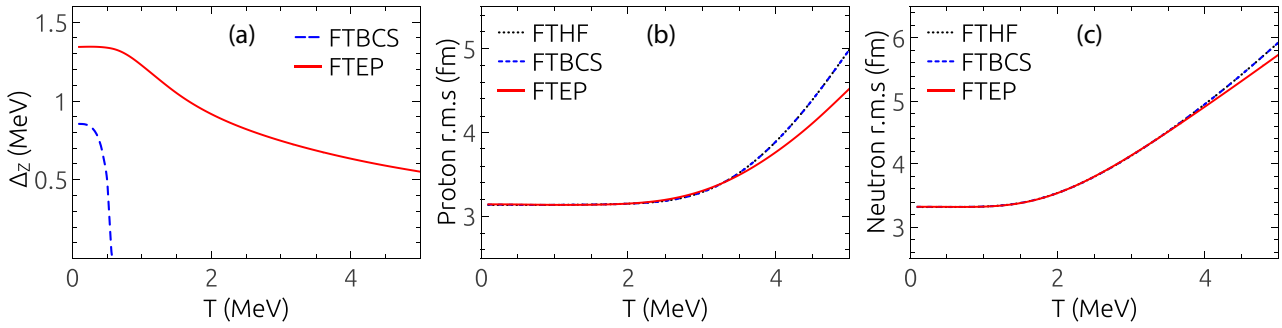

FIG. 4. Proton pairing gaps (a) and root-mean-square (rms) radii for protons (b) and neutrons (c) in ^{34}Si obtained within the FTHF, FTBCS, and FTEP at $T \neq 0$.

the deviation of the HFB predictions from the experimental two-nucleon separation energies is much larger.

Also shown in Table I are the values of the depletion factor, which is defined as

$$F = \frac{\rho_{\max} - \rho_{\text{cent}}}{\rho_{\max}}, \tag{26}$$

where $\rho_{\max}$ and ρ_{cent} are the values of the nucleon density at its maximum and at the nuclear center ($r = 0$), respectively. In the presence of pairing, the depletion in the central region of the proton density at $T = 0$ is predicted within the FTEP and HFB [29] as $F \simeq 15\%$ by using the BSk14 interaction. This value is smaller than that obtained in our calculations ($F \simeq 19\%$ within the FTBCS and FTEP by using the MSk3 interaction), whereas the FTHF produces $F \simeq 24\%$. These comparisons indicate that pairing, employed in the HFB calculations in Refs. [9,29], is stronger than that used in our calculations for ^{34}Si, which is assumed as a doubly magic nucleus. Once again, it also shows that, for this nucleus the MSk3 interaction is more suitable than the BSk14 one (see Table II).

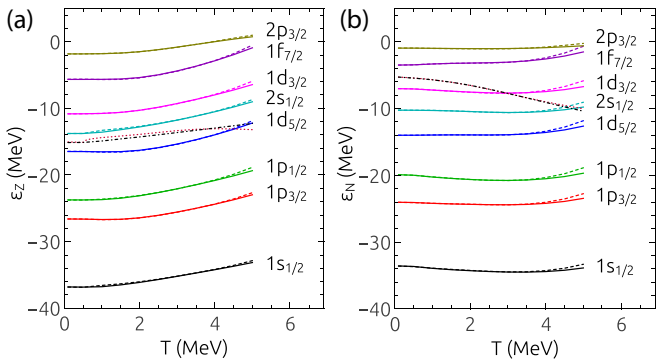

FIG. 5. Single-particle energies for protons (a) and neutrons (b) in ^{34}Si obtained within the FTEP (solid lines) and FTBCS (dashed lines) as functions of temperature. The dash-dotted line in (a) is the exact proton chemical potential, obtained as $\lambda^{(N)} = [\mathcal{F}(N+2,T) + \mathcal{F}(N-2,T)]/4$, where $\mathcal{F}(N \pm 2, T)$ are the exact free energies of the systems with $N \pm 2$ protons, whereas the dotted line in (a) is the proton chemical potential obtained within the FTBCS. The dotted and dash-dotted lines in (b) are the chemical potential obtained within the IPM calculation (without pairing) using the neutron single-particle spectra obtained within the FTBCS and FTEP, respectively.

A number of zero values of the depletion factor F for ^{22}O shown in the 7th column in Table I indicate that the existence of the bubble in this nucleus depends on the interaction. In particular, the calculations by using a number of MSk and BSk interactions such as MSk4-MSk8, BSk1, BSk3, and BSk18 do not produce the neutron bubble in ^{22}O, whereas those carried out within the FTEP by using all of the MSk and BSk interactions always predict the proton bubble in ^{34}Si. This also indicates that ^{34}Si is very likely to be a bubble nucleus. Although both the MSk3 and BSk14 interactions reproduce the binding and two-neutron separation energies, the corresponding depletion factors $F \simeq 2\%$ and 7% obtained within the FTEP at $T = 0$ are quite different. Meanwhile, the HFB results [9,29], which fail to describe the two-nucleon separation energies because the binding energies do not completely match the experimental data (Fig. 1), show the depletion factor $F \simeq 3\%$ and 4% for the SLy4 and BSk14 (or D1S) interactions, respectively (see Table II). Our prediction also shows a significant difference with the RMF+BCS which produces the depletion factor $F = 17\%$ by using a very small pairing (see Table II and also Table 2 in Ref. [11]).

B. Zero temperature

Shown in Fig. 2 are the proton densities ρ_Z in ^{34}Si obtained within the FTHF, FTBCS, FTEP (by using the Skyrme MSk3) and FTEP-BSk14 (by using the Skyrme BSk14) at $T = 0$ in comparison with the HFB predictions taken from Ref. [29] by using the Skyrme BSk14. All the calculations reveal the bubble structure as the depletion of ρ_Z at $r = 0$. Among them the HFB predicts a shallowest bubble.

The neutron densities $\rho_N(r)$ obtained for ^{22}O within the same approaches are displayed in Fig. 3 in comparison with the predictions of the HFB calculations [29]. The results shown in Fig. 3 and Table II indicate that the bubbles, predicted within the FTBCS and FTEP, are much shallower (the depletion factor $F = 2\%$) as compared to the predictions of the FTHF ($F \simeq 11\%$), where pairing is absent, whereas for other calculations, F varies from 4% to 34%. The reason comes from the fact that the neutron-rich ^{22}O nucleus is not a doubly magic nucleus, and is lighter than ^{34}Si. Therefore the pairing correlation in this nucleus is stronger than that of ^{34}Si. These features increase the $2s_{1/2}$ occupancy of ^{22}O to a value sufficiently large (about 0.25 within the FTEP and FTBCS) so that the bubble structure is

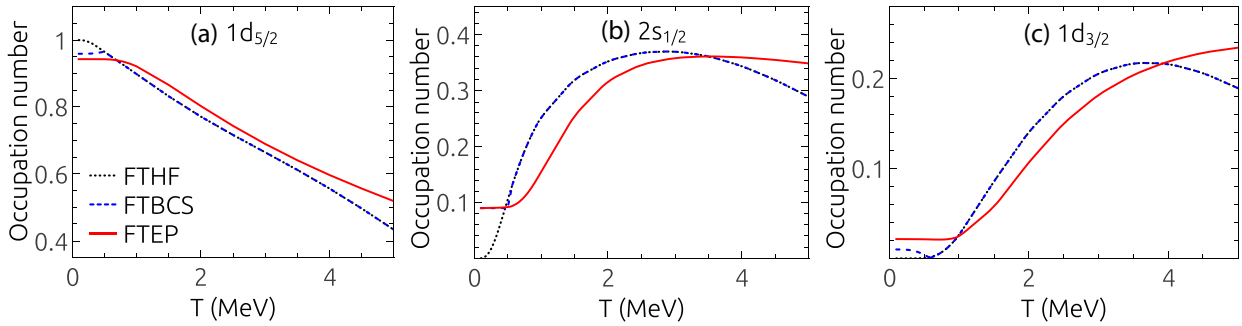

FIG. 6. Occupation numbers of proton single-particle levels $1d_{5/2}$ (a), $2s_{1/2}$ (b), and $1d_{3/2}$ (c) in ^{34}Si obtained within FTHF, FTBCS, and FTEP.

almost washed out at $T = 0$. The HFB calculations in Ref. [9] assume that ^{22}O behaves almost as a doubly magic nucleus so that, although pairing is included, it turns out to be too weak to overcome this assumed double magicity. The relativistic HFB calculations by using the density-dependent interaction DDME2 even result in a deeper bubble for ^{22}O as shown in Fig. 8 of the same paper.

C. Finite temperature

Given the clear proton bubble structure, ^{34}Si is chosen as the typical candidate, which can be used to study the evolution of the bubble at $T \neq 0$. In general, it is naturally expected that temperature will eventually wash out the bubble structure as it increases the occupation number of the unoccupied $2s_{1/2}$ level. However, the increase of temperature also leads to the quenching of the pairing gap, so the competition of the two effects in different approaches may lead to different values of temperature, at which the bubble structure is washed out. The present section will analyze in detail these features.

Shown in Fig. 4(a) are the proton pairing gaps in ^{34}Si obtained within the FTBCS and FTEP as functions of T. The FTBCS gap collapses at the critical temperature $T_c \simeq 0.57$ MeV, whereas the FTEP gap remains finite at T as high as 5 MeV. This nonvanishing FTEP proton gap at high T significantly affects the proton root-mean-square (rms) radius of ^{34}Si, as shown in Fig. 4(b), slowing down its increase with T at $T > 2$ MeV. This should be compared with the sharp increase predicted by the FTBCS, which is identical to the prediction of the FTHF because the FTBCS gap is zero in this temperature region. Regarding the neutron rms radius, given the absence of the neutron pairing gap in this neutron closed-shell nucleus, the three methods predict nearly the same result as can be seen in Fig. 4(c). A slight difference between the neutron rms radii obtained within the FTBCS (FTHF) and FTEP at $T > 2$ MeV comes from the difference between the FTBCS and FTEP proton pairings, which affects not only the proton but also the neutron parts of the HF potential and the wave functions. Both the neutron and proton rms radii increase with T, in agreement with the results of Refs. [65,66]. The proton single-particle energies obtained within the FTEP are more strongly affected by the temperature, resulting in their stronger increase with T as compared to that of the neutron ones as seen in Fig. 5.

Shown in Fig. 6 are the occupation numbers of three proton single-particle levels closest to the Fermi surface, namely $1d_{5/2}$ (a), $2s_{1/2}$ (b), and $1d_{3/2}$ (c), obtained within the FTHF, FTBCS, and FTEP for ^{34}Si. The occupation number of the $1d_{5/2}$ level

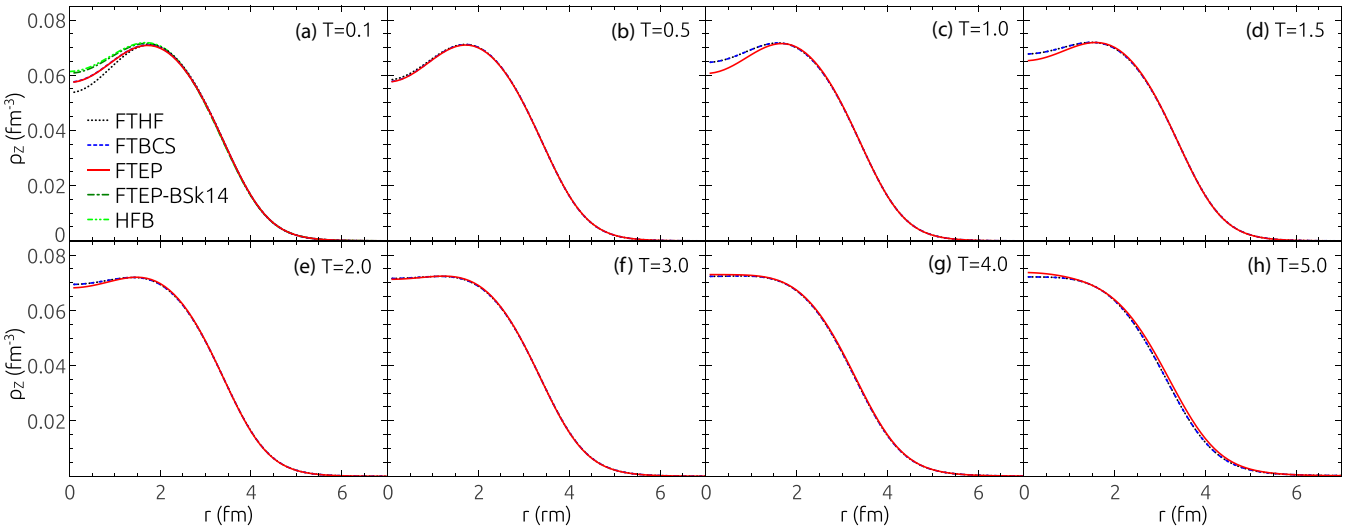

FIG. 7. Proton density $\rho_Z(r)$ in ^{34}Si obtained within the FTHF, FTBCS, and FTEP at several temperatures.

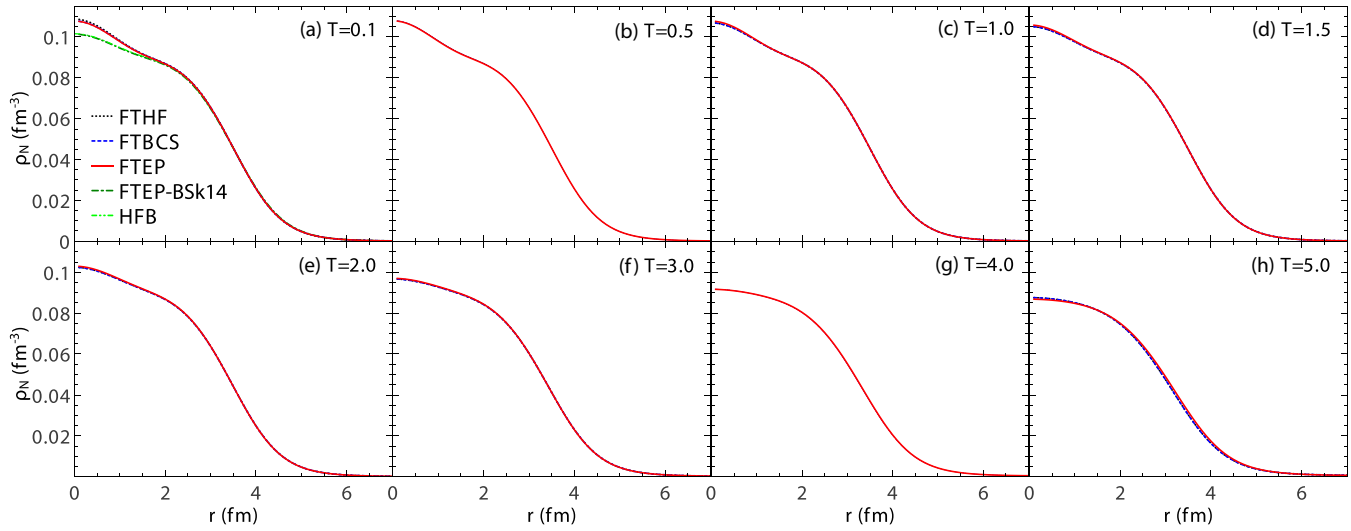

FIG. 8. Neutron density $\rho_N(r)$ in ^{34}Si obtained within the FTHF, FTBCS, and FTEP at several temperatures.

decreases with increasing T, whereas those of the other two levels increase with T. Because pairing is absent within the FTHF, $f_{1d_{5/2}}$ decreases from its value equal to 1 at $T = 0$ to about 0.43 at $T = 5$ MeV, whereas $f_{2s_{1/2}}$ ($f_{1d_{3/2}}$) increases from 0 at $T = 0$ to about 0.29 (0.19) at $T = 5$ MeV. The occupation numbers obtained within the FTBCS are different from the FTHF ones at $T < T_c$ because of the FTBCS pairing gap in this temperature region. Within the FTEP, pairing is always present in the whole temperature region as seen in Fig. 4(a), so the occupation numbers of the levels below (above) the Fermi surface obtained within the FTEP decrease (increase) much slower than those obtained within the FTHF and FTBCS.

The proton and neutron density profiles in ^{34}Si at several temperatures are plotted in Figs. 7 and 8, respectively. At $T = 0$, the bubble structure is clearly seen in the proton densities obtained within the three methods. The bubble structure predicted within the FTHF, which produces the occupation number of the $2s_{1/2}$ level equal to 0, is more pronounced (deeper) than those predicted by the FTBCS and FTEP, in which the pairing interaction G is adjusted to reproduce the experimental binding energy and the value of $f_{2s_{1/2}}$ equal to 0.09 as was discussed previously (see the third line and second column in Table I). As $f_{2s_{1/2}}$ increases with T, the bubble structure predicted within the three methods becomes shallower and gradually disappears at $T = T_F$. It can also be seen here that exact pairing keeps the proton central density less sensitive to the change of temperature. Indeed, as T increases from 0.1 to 2 MeV, $\rho_Z(r)$ predicted by the FTHF and FTBCS increase from around 0.054 and 0.058 to 0.069 fm^{-3}, whereas within the FTEP this increase is from 0.058 to 0.068 fm^{-3}, resulting in a disappearance of the bubble structure at a lower $T_F^{\rm FTEP} \simeq 4$ MeV as compared to the value $T_F^{\rm FTBCS} \simeq 4.5$ MeV predicted by the FTBCS, which coincides with the FTHF at $T \geqslant T_c$. These values of T_F are confirmed by Fig. 9, which shows the depletion factor F as a function of T. The disappearance of bubble structure at these temperatures can also be seen in the density

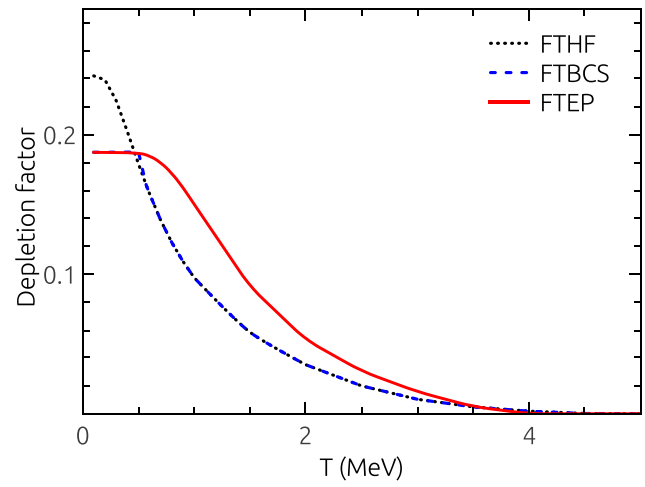

FIG. 9. Depletion factor F for the proton density $\rho_Z(r)$ obtained within the FTHF, FTBCS, and FTEP for ^{34}Si.

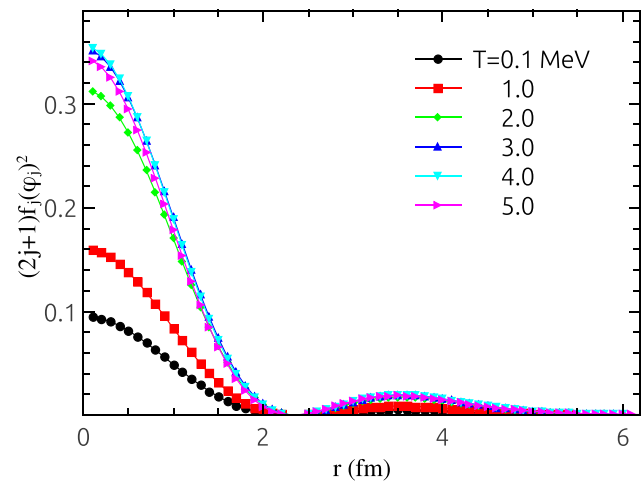

FIG. 10. Wave function of the proton $2s_{1/2}$ level in ^{34}Si obtained within the FTEP at several temperatures.

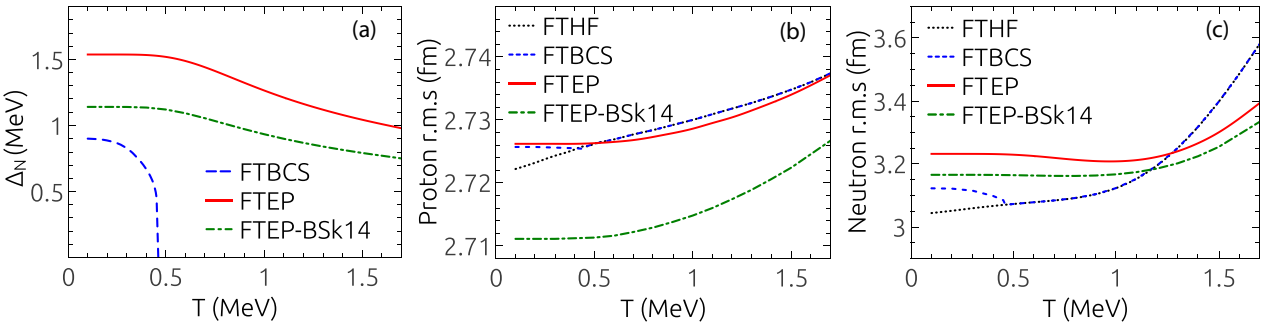

FIG. 11. Neutron pairing gaps (a) and root-mean-square (rms) radii for protons (b) and neutrons (c) in ^{22}O obtained within the FTHF, FTBCS, and FTEP.

profiles shown in Figs. 7(f) and 7(g). These results indicate that the bubble structure in ^{34}Si should completely disappear when the occupation number of $2s_{1/2}$ level reaches a value of about ∼0.35. They also demonstrate that, owing to the double magicity, the pairing effect in ^{34}Si is not sufficiently large to cause a significant difference between the FTBCS and FTEP results.

The evolution of the bubble structure in ^{34}Si can be explained in more detail by looking at the wave function of the $2s_{1/2}$ proton level shown in Fig. 10. As mentioned in the introduction, the s-radial wave has a special character, which is the pronounced maximum located at the nuclear center $r = 0$. If this s-radial wave is absent or its contribution (occupation number) to the total wave function is somewhat small, the bubble structure will appear and vice versa. This feature is clearly seen in Fig. 10 in which the maximum of the wave function of $2s_{1/2}$ proton level at $r = 0$ is around 0.1 at $T = 0.1$ MeV and increases with T, leading to the gradual disappearance of the bubble structure in this nucleus. Regarding the neutron density of ^{34}Si, no bubble structure is seen even at $T = 0$ as the $2s_{1/2}$ neutron level is located below the Fermi surface [see, e.g., Fig. 5(b)], leading to a very large value of the corresponding occupation number.

As ^{22}O shows a very shallow bubble structure at $T = 0$, its disappearance is expected to happen at low T. In this nucleus, we used the MSk3 interaction to carry out the calculations within the FTHF, FTBCS, and FTEP and also the BSk14 one within the FTEP. When the MSk3 interaction is used, the strong pairing effect at $T = 0$ produces a relatively large $2s_{1/2}$ occupation number of neutron (about 0.25 within the FTBCS and FTEP). The collapse of the FTBCS pairing gap at the critical temperature $T_c = 0.46$ MeV [Fig. 11(a)] leads to a bending in the FTBCS curves in Figs. 11(b), 11(c), and 12 at T_c. In Figs. 11(b) and 11(c), because of the temperature effect, the nucleon root-mean-square radii of ^{22}O also increase as expected. The difference of neutron r.m.s within the FTBCS and FTEP is much larger than the difference of proton r.m.s. The explanation comes from the strong pairing effect in the open neutron shell of ^{22}O. Therefore, this phenomenon is observed more clearly than what occurs in the doubly magic ^{34}Si nucleus. At $1 < T < 2$ MeV, because of the nonvanishing FTEP gap, the neutron r.m.s within the FTEP slowly increases as compared to that predicted by the FTBCS. A similar feature is seen in Fig. 12 for the single-particle occupation numbers. As T increases, the closed-shell proton density remains almost unchanged [Figs. 13(a1)–13(a3)]. Meanwhile, the bubble structure in the neutron density is washed out at $T_F = 0.57$ MeV within the FTHF and FTBCS, and at $T_F = 0.85$ MeV within the FTEP [Figs. 13(b1)–13(b3) and 14(a) and 14(b)]. Because of the neutron unclosed shell and the quenching of the BCS pairing gap at T_c, the value $T_F^{\rm FTBCS}$ is smaller than $T_F^{\rm FTEP}$. At these temperatures, the occupation number of the $2s_{1/2}$ level takes the values equal to 0.33 and 0.32 within FTBCS and FTEP, respectively, which are fully consistent with the FTEP nonvanishing pairing gap.

When the BSk14 interaction is used, the FTEP predicts a deeper neutron bubble than that obtained by using the MSk3 interaction in ^{22}O (Fig. 3) at $T = 0$. The $2s_{1/2}$ occupation number is equal to 0.14 with a smaller pairing gap $\Delta_N = 1.14$ MeV as compared to the gap of 1.54 MeV obtained by using

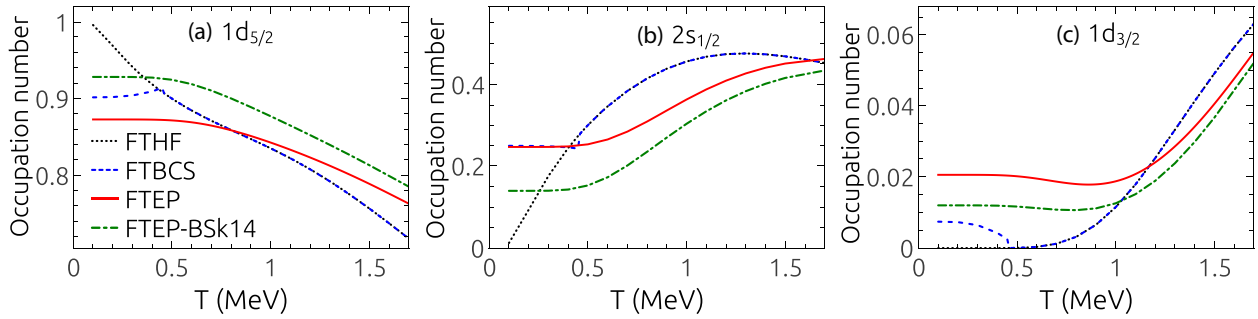

FIG. 12. Occupation numbers of proton single-particle levels $1d_{5/2}$ (a), $2s_{1/2}$ (b), and $1d_{3/2}$ (c) in ^{22}O obtained within FTHF, FTBCS, and FTEP.

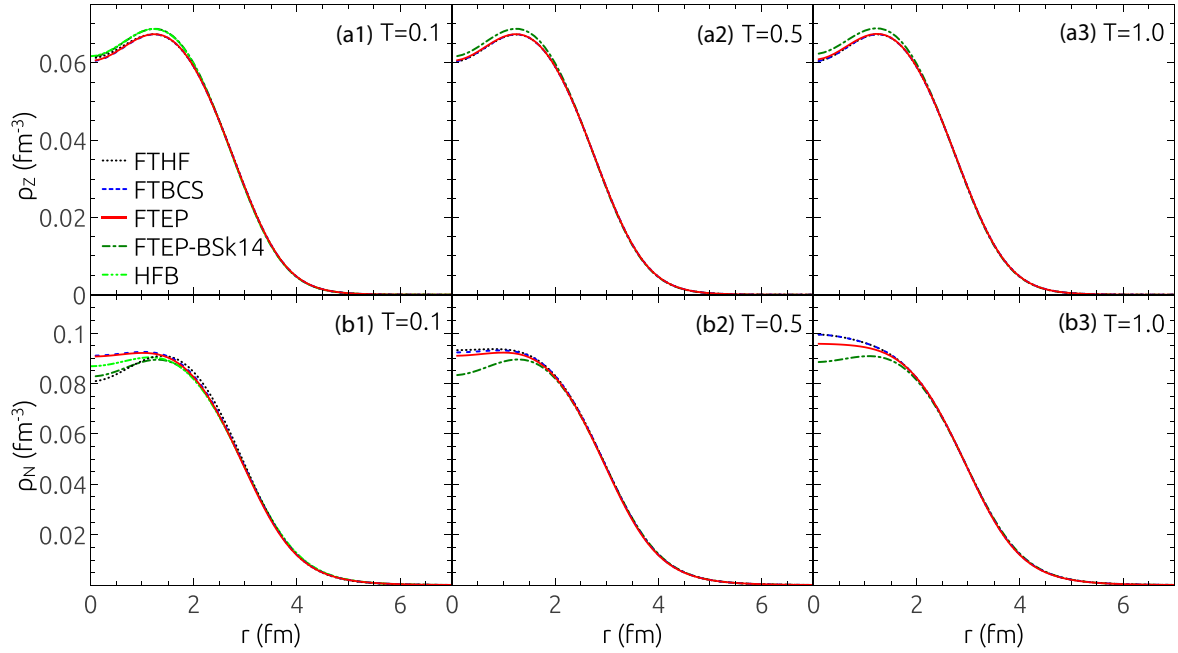

FIG. 13. Proton [(a1)–(a3)] and neutron [(b1)–(b3)] densities in ^{22}O obtained within the FTHF, FTBCS, and FTEP at several temperatures.

the MSk3 interaction (see Figs. 11(a) and [12]). Consequently, the bubble vanishes at a higher critical temperature $T_F = 1.7$ MeV (Fig. 14). The $2s_{1/2}$ occupation number at this temperature is equal to 0.43. With increasing T, the r.m.s of the proton and neutron have the same behavior but their values are lower than those predicted by using the MSk3 interaction [Figs. 11(b) and 11(c)] because of weaker pairing.

IV. CONCLUSIONS

The present paper studies the bubble structures of ^{22}O and ^{34}Si nuclei at zero and finite temperatures within the Skyrme Hartree-Fock mean field, which consistently incorporates the superfluid pairing. The latter is obtained within the finite-temperature BCS theory (FTBCS) and the exact solutions of the pairing Hamiltonian at finite temperature T (FTEP). The results obtained by using a series of BSk and MSk interactions show the existence of proton bubble structure in ^{34}Si at zero temperature in all cases, whereas the neutron bubble in ^{22}O does not shows up in the cases using the MSk4–MSk8, BSk1, BSk3, and BSk18 interactions. This indicates that the existence of the neutron bubble in this nucleus is inconclusive as it depends on the interaction. The only way to resolve this ambiguity in ^{22}O is to know the experimentally extracted occupation number of its $2s_{1/2}$ level. By using the MSk3 interaction, our calculations within the FTEP reproduce well the binding energies and two-proton (neutron) separation energies of these nuclei. The bubble structure exists at $T = 0$ in both ^{22}O and ^{34}Si. The proton bubble in ^{34}Si, which appears because of a very low occupancy of the $2s_{1/2}$ level, becomes less pronounced as T increases and completely disappears when T reaches a critical value T_F of around 4 MeV, at which the depletion factor vanishes. The evolution of neutron bubble in ^{22}O is similar. However, this bubble structure disappears at different values of the critical temperature T_F within three different microscopic methods. Because of the nonvanishing FTEP pairing gap, the value $T_F = 0.85$ MeV, predicted by the FTEP for the neutron bubble disappearance in ^{22}O, is significantly higher than that obtained within the FTBCS

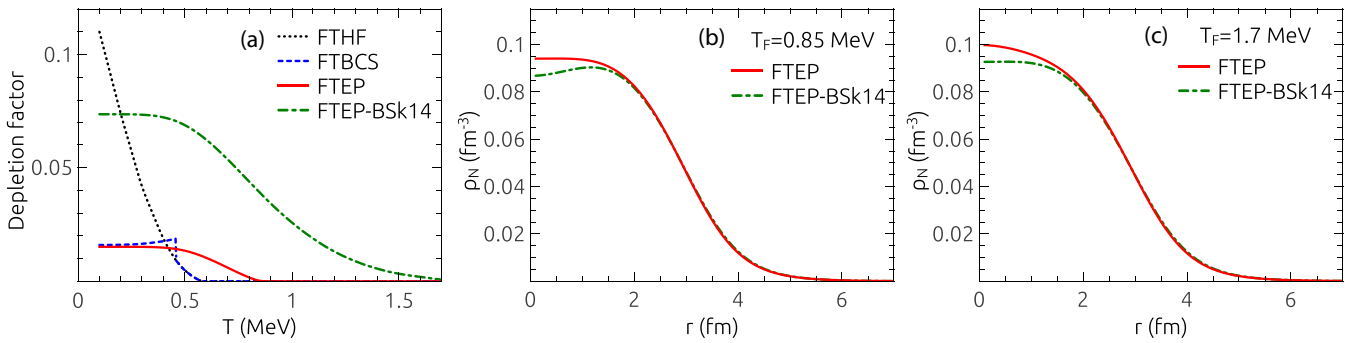

FIG. 14. (a): Depletion factor F for the neutron densities ρ_N in ^{22}O obtained within the FTHF, FTBCS, and FTEP. (b) and (c) Same as in Fig. 13 but at two critical temperatures T_F correspond to the FTEP calculations which are carried out for the MSk3 and BSk14 interaction.

(0.57 MeV). This phenomenon does not occur in ^{34}Si, which is assumed to be a doubly magic nucleus with weak pairing instead of the neutron-rich ^{22}O nucleus with strong pairing. The results obtained also show that the bubble structures in ^{22}O and ^{34}Si completely disappear when the occupation number of the $2s_{1/2}$ level reaches a value higher than 0.32 and 0.35, respectively. The BSk14 interaction is also used to study the neutron bubble in ^{22}O only within the FTEP. The results of our calculations show a deeper bubble structure than that obtained by using the MSk3 interaction, which disappears at $T_F = 1.7$ MeV because of the small pairing. In general, our calculations show a stronger pairing effect in ^{22}O and weaker one in ^{34}Si as compared to the predictions in Refs. [9,29]. Exact pairing also makes the central neutron density in ^{22}O less sensitive to the change of temperature in the interval $0 \leqslant T \leqslant 1$ MeV.

ACKNOWLEDGMENTS

L.T.P. acknowledges the International Internship Program at RIKEN, where this work was initiated. The FORTRAN IMSL Library by Visual Numerics on the RIKEN supercomputer HOKUSAI-GreatWave System was used in the numerical calculations. This work is funded by the National Foundation for Science and Technology Development (NAFOSTED) of Vietnam through Grant No. 103.04-2017.69.

[1] H. A. Wilson, Phys. Rev. **69**, 538 (1946).
[2] P. J. Siemens and H. A. Bethe, Phys. Rev. Lett. **18**, 704 (1967).
[3] X. Campi and D. W. L. Sprung, Phys. Lett. B **46**, 291 (1973).
[4] C. Y. Wong, Phys. Lett. B **41**, 451 (1972).
[5] C. Y. Wong, Ann. Phys. **77**, 279 (1973).
[6] O. Bohigas, X. Campi, H. Krivin, and J. Treiner, Phys. Lett. **64**, 381 (1976).
[7] J. Friedrich and N. Voegler, Nucl. Phys. A **459**, 10 (1986).
[8] E. Khan, M. Grasso, J. Margueron, and N. Van Giai, Nucl. Phys. A **800**, 37 (2008).
[9] M. Grasso, L. Gaudefroy, E. Khan, T. Niksic, J. Piekarewicz, O. Sorlin, N. Van Giai, and D. Vretenar, Phys. Rev. C **79**, 034318 (2009).
[10] J.-M. Yao, S. Baroni, M. Bender, and P.-H. Heenen, Phys. Rev. C **86**, 014310 (2012).
[11] G. Saxena *et al.*, Int. J. Mod. Phys. E **26**, 1750072 (2017).
[12] K. Dietrich and K. Pomorski, Nucl. Phys. A **627**, 175 (1997).
[13] M. Bender, K. Rutz, P.-G. Reinhard, J. A. Maruhn, and W. Greiner, Phys. Rev. C **60**, 034304 (1999).
[14] J.-F. Berger, L. Bitaud, J. Dechargé, M. Girod, and K. Dietrich, Nucl. Phys. A **685**, 1c (2001).
[15] J. Dechargé, J.-F. Berger, M. Girod, and K. Dietrich, Nucl. Phys. A **716**, 55 (2003).
[16] W. J. Swiatecki, Phys. Scr. **28**, 349 (1983).
[17] J. C. Pei, F. R. Xu, and P. D. Stevenson, Phys. Rev. C **71**, 034302 (2005).
[18] J. M. Cavedon, B. Frois, D. Goutte, M. Huet, P. Leconte, C. N. Papanicolas, X.-H. Phan, S. K. Platchkov, S. Williamson, W. Boeglin, and I. Sick, Phys. Rev. Lett. **49**, 978 (1982).
[19] V. R. Pandharipande *et al.*, Rev. Mod. Phys. **69**, 981 (1997).
[20] L. Zamick, V. Klemt, and J. Speth, Nucl. Phys. A **245**, 365 (1975); A. Covello and G. Sartoris, *ibid.* **93**, 481 (1967); N. Azziz and A. Covello, *ibid.* **123**, 681 (1969).
[21] B. G. Todd-Rutel, J. Piekarewicz, and P. D. Cottle, Phys. Rev. C **69**, 021301(R) (2004).
[22] Y. Chu, Z. Ren, Z. Wang, and T. Dong, Phys. Rev. C **82**, 024320 (2010).
[23] M. Grasso *et al.*, Int. J. Mod. Phys. E **18**, 2009 (2009).
[24] A. Mutschler *et al.*, Nat. Phys. **13**, 152 (2017).
[25] J. M. Yao, H. Mei, and Z. P. Li, Phys. Lett. B **723**, 459 (2013).
[26] M. Beiner and R. J. Lombard, Phys. Lett. B **47**, 399 (1973).
[27] D. Vautherin and D. M. Brink, Phys. Rev. C **5**, 626 (1972).
[28] P. Ring and P. Schuck, *The Nuclear Many-Body Problem* (Springer-Verlag, Berlin/Heidelberg, 2004).
[29] https://www-nds.iaea.org/RIPL-3/
[30] K. Langanke, J. A. Maruhn, and S. E. Koonin, *Computational Nuclear Physics 1* (Springer-Verlag, Berlin/Heidelberg, 1990).
[31] G. Colo, L. Cao, N. V. Giai, and L. Capelli, Comput. Phys. Commun. **184**, 142 (2013).
[32] J. Dobaczewski, W. Nazarewicz, and P.-G. Reinhard, Nucl. Phys. A **693**, 361 (2001).
[33] A. Volya, B. A. Brown, and V. Zelevinsky, Phys. Lett. B **509**, 37 (2001).
[34] V. Zelevinsky and A. Volya, Phys. At. Nucl. **66**, 1781 (2003).
[35] A. Bohr and B. Mottelson, *Nuclear Structure* (Benjamin, New York, 1974), Vol. 2.
[36] D. M. Brink and R. A. Broglia, *Nuclear Superfluidity* (Cambridge University Press, Cambridge, 2004).
[37] J. Bardeen, L. N. Cooper, and J. R. Schrieffer, Phys. Rev. **106**, 162 (1957); **108**, 1175 (1957).
[38] T. Alm, B. L. Friman, G. Ropke, and H. Schulz, Nucl. Phys. A **551**, 45 (1993).
[39] E. Khan, N. Van Giai, and N. Sandulescu, Nucl. Phys. A **789**, 94 (2007).
[40] N. Quang Hung and N. Dinh Dang, Phys. Rev. C **79**, 054328 (2009).
[41] N. Dinh Dang and N. Quang Hung, Phys. Rev. C **77**, 064315 (2008).
[42] L. G. Moretto, Phys. Lett. B **40**, 1 (1972).
[43] A. L. Goodman, Nucl. Phys. A **352**, 30 (1981).
[44] N. Dinh Dang, P. Ring, and R. Rossignoli, Phys. Rev. C **47**, 606 (1993).
[45] N. Dinh Dang and A. Arima, Phys. Rev. C **68**, 014318 (2003); N. Dinh Dang, *ibid.* **76**, 064320 (2007).
[46] N. Quang Hung, N. Dinh Dang, and L. T. Quynh Huong, Phys. Rev. Lett. **118**, 022502 (2017).
[47] O. Burglin and N. Rowley, Nucl. Phys. A **602**, 21 (1996).
[48] H. Molique and J. Dudek, Phys. Rev. C **56**, 1795 (1997).
[49] P. G. Reinhard, F. Grummer, and K. Goeke, Z. Phys. A **317**, 339 (1984).
[50] M. Bender, K. Rutz, P.-G. Reinhard, and J. Maruhn, Eur. Phys. J. A **7**, 467 (2000).
[51] M. Samyn *et al.*, Nucl. Phys. A **700**, 142 (2002).
[52] S. Goriely, M. Samyn, P.-H. Heenen, J. M. Pearson, and F. Tondeur, Phys. Rev. C **66**, 024326 (2002).
[53] M. Samyn, S. Goriely, and J. M. Pearson, Nucl. Phys. A **725**, 69 (2003).
[54] S. Goriely, M. Samyn, M. Bender, and J. M. Pearson, Phys. Rev. C **68**, 054325 (2003).

[55] M. Samyn, S. Goriely, M. Bender, and J. M. Pearson, Phys. Rev. C **70**, 044309 (2004).
[56] S. Goriely, M. Samyn, J. M. Pearson, and M. Onsi, Nucl. Phys. A **750**, 425 (2005).
[57] S. Goriely, M. Samyn, and J. M. Pearson, Nucl. Phys. A **773**, 279 (2006).
[58] S. Goriely, M. Samyn, and J. M. Pearson, Phys. Rev. C **75**, 064312 (2007).
[59] S. Goriely and J. M. Pearson, Phys. Rev. C **77**, 031301 (2008).
[60] N. Chamel, S. Goriely, and J. M. Pearson, Nucl. Phys. A **812**, 72 (2008).
[61] S. Goriely, N. Chamel, and J. M. Pearson, Phys. Rev. Lett. **102**, 152503 (2009).
[62] N. Chamel, S. Goriely, and J. M. Pearson, Phys. Rev. C **80**, 065804 (2009).
[63] F. Tondeur, S. Goriely, J. M. Pearson, and M. Onsi, Phys. Rev. C **62**, 024308 (2000).
[64] S. Goriely, M. Pearson, and F. Tondeur, Nucl. Phys. A **688**, 349 (2001).
[65] P. Bonche, S. Levit, and D. Vautherin, Nucl. Phys. A **436**, 265 (1985).
[66] A. N. Antonov, D. N. Kadrev, M. K. Gaidarov, P. Sarriguren, and E. M. de Guerra, Phys. Rev. C **95**, 024314 (2017).